RSC Advances

PAPER

Cite this: *RSC Adv.*, 2019, **9**, 7747

A microwave-activated coal fly ash catalyst for the oxidative elimination of organic pollutants in a Fenton-like process†

Nannan Wang, *[ab] Han Xu[a] and Shuo Li*[c]

Raw coal fly ash was first activated by microwave irradiation to promote its catalytic potential and then used as a Fenton-like catalyst to treat polyacrylamide-contaminated wastewater. The optimal activation conditions of the raw coal fly ash (microwave power = 700 W, irradiation time = 10 min, mixing speed = 120 rpm, and raw coal fly ash loading = 20 g L^{-1}) were determined by the orthogonal test. The significance of each effective parameter follows the order: raw coal fly ash loading > microwave power > irradiation time > mixing speed. Microwave irradiation can change the surface morphology and remarkably increase the specific surface area and pore volume. More than 75% of the TOC in the polyacrylamide-contaminated wastewater can be removed under the optimized treatment conditions ([H_2O_2] = 12 mg L^{-1}, catalyst loading = 10 g L^{-1}, [polyacrylamide] = 200 mg L^{-1}, T = 313 K). The kinetic study shows that the variation in the catalyst loading and the polyacrylamide concentration can change the degradation path of the polyacrylamide, whereas the variation in the H_2O_2 dosage can accelerate the degradation of polyacrylamide. The Fenton-like process studied herein has a wider optimal pH range (2–5) than that of the classic Fenton process (3). The catalyst has weak catalytic capacity but better catalytic persistence than that of Fe^{2+}. During the five runs of the catalyst, some heavy metallic and toxic elements (Fe, Al, Ti, Cr, Mn, *etc.*) can be detected but under the limits of the GB8978-1996 standard. Leaching can weaken the catalytic capacity (*i.e.*, stability) of the catalyst. The catalytic process is caused by the synergism of multiple metals and consists of heterogeneous and homogeneous processes.

Received 1st February 2019
Accepted 21st February 2019

DOI: 10.1039/c9ra00875f

rsc.li/rsc-advances

Introduction

The Fenton process, as a wastewater treatment process, is well known because of the generation of $^{\cdot}OH$ (2.8 V of redox potential *versus* the normal hydrogen electrode) *via* the reaction (1)[1]

$$Fe^{2+} + H_2O_2 \rightarrow Fe^{3+} + OH^- + {}^{\cdot}OH \quad (1)$$

However, the optimal pH (approx. 3)[2] and the generation of sludge containing the Fe element[3] limit the application of the Fenton process.

Exploring a new catalyst to replace Fe^{2+} is a widely recognized solution to remove this limitation.[4] Some catalysts have been synthesized such as Z-scheme Fe_2O_3-doped Cu_2O, Fe^{3+}–Al_2O_3, $CoFe_2O_4$ powder, Pd–Fe_3O_4, $CoM_xFe_{2-x}O_4$, Fe–Ti pillared bentonite, $Fe_{73.5}Si_{13.5}B_9Cu_1Nb_3$, and Fe–Mn-sepiolite.[5–11] All these catalysts can effectively catalyze the above reaction. It is valuable to notice that these catalysts have an identical feature, *i.e.*, they contain the Fe element and some auxiliary metallic elements such as Cu, Al, Co, Pd, Mn, Ti, and/or Nb. However, the preparation cost of these catalysts is high and the source of raw materials is limited. Thus, exploring a cheaper catalyst is encouraged.

Coal fly ash (CFA), as a well-known environmental pollutant, could be an appropriate alternative because of its distinctive features: (1) contains Fe element and other elements that are always doped on the synthesized Fenton-like catalyst; (2) can cause serious environmental pollution and exploring new methods to reuse it are urgent; (3) exists widely, easy to purchase, and its price is low. In the scientific research history of CFA, it has been studied in some research fields such as soil improvement, metal extraction, and preparation of zeolite/adsorbent.[12–15] Relatively speaking, the use of a Fenton-like catalyst after an appropriate activation to treat organic wastewater has not attracted enough attention until now. CFA has been reported to absorb electromagnetic waves because of the existence of ferromagnetic material and other metallic oxides.[16] However, this property was never noticed in the preparation of Fenton-like catalysts based on CFA.

[a]*Department of Environmental Engineering, Beijing Institute of Petrochemical Technology, Beijing 102617, PR China. E-mail: wnn_flying@163.com*
[b]*Beijing Key Laboratory of Pipeline Critical Technology and Equipment for Deepwater Oil & Gas Development, Beijing 102617, PR China*
[c]*College of Chemistry and Chemical Engineering, Qiqihar University, Qiqihar, 161006, PR China. E-mail: shuo_105@163.com*

† Electronic supplementary information (ESI) available. See DOI: 10.1039/c9ra00875f

Microwave (MW) is a wavelength band (300 MHz to 300 GHz) of the electromagnetic spectrum. It has distinctive thermal and non-thermal effects.[2] As for the thermal effect, MW can penetrate into (or pierce through) some materials (such as metallic oxides) and heat materials throughout their volume simultaneously. This heating mode exhibits a distinction compared with the traditional heating. As for the non-thermal effect, MW can excite the reactant molecules to the higher vibrational and rotational energy levels. MW has been used widely in chemical reactions depending on the ability of accelerating the reaction rate, reducing the activation energy, and strengthening the vibration of chemical bonds.[17]

In recent years, polyacrylamide (PAM) has been used widely in the enhanced oil recovery process as it can increase the bulk viscosity and improve the oil–water mobility ratio.[18] However, the generated polymer-flooding wastewater (PFW) has caused serious production pressure and environmental issues in China. The PAM in the PFW can enhance the stability of the oil–water emulsion, which makes it difficult to treat the PFW by conventional methods.[19] Nowadays, part of the PFW is being injected back into the stratum and the rest is discharged directly into natural water and/or soil, thus causing water and soil pollution. Therefore, the removal of PAM from PFW is a critical step in the effective treatment of PFW before efflux.

In this work, raw CFA (CFA_R) was chosen as the raw material of a Fenton-like catalyst, synthetic PAM wastewater was chosen as the target pollutant, and a Fenton-like process catalyzed by MW-activated CFA (denoted by CFA_{MW}) was chosen to treat the PAM wastewater. Firstly, the activation condition of the CFA_R was optimized and the CFA_{MW} was characterized by SEM, BET, XRD, XRF, and FTIR. After that, the treatment conditions of the PAM wastewater were optimized and the degradation kinetics of PAM was analyzed. Subsequently, the features of the Fenton-like process (optimal pH range, leachability, and stability of CFA_{MW}) were investigated and discussed. Finally, the catalytic mechanism of CFA_{MW} was proposed. This work gives a new activation method for CFA_R and provides an idea on how to minimize the pollution from CFA and PFW.

Materials and methods

Chemical reagents

PAM (analytical grade, molecular weight = 3.0×10^6) and H_2O_2 were purchased from Sigma-Aldrich, while HCl and NaOH were purchased from Honeywell. H_2O_2 was stored in the dark at 277 K. All chemical reagents were prepared using 18 MΩ cm Milli-Q water (MQ). All used glassware were soaked in an alcohol solution for at least 24 h and washed with MQ before use.

The CFA_R was obtained from a coal-fired power plant in China. The electromagnetic parameters of the CFA_R are shown in Table 1. It was washed by MQ before the experiments to remove the impurities and dried at 378 K.

Preparation of CFA_{MW}

The MW activation process of CFA_R was conducted in a retrofitted MW oven (EM-202MS1, SANYO, Japan, Fig. 1). A certain amount of CFA_R was tiled on the multi-layer plate in the preparation chamber. The MW and the vibratory rod were switched on simultaneously and the activation process was started. The vibration of the chamber can force the CFA_R to disperse in the whole space of the preparation chamber and to receive adequate MW irradiation. After the activation, the prepared CFA catalyst (*i.e.*, CFA_{MW}) was stored in a drying basin.

Table 1 Electromagnetic parameters of CFA_R used in this work[a]

Frequency/GHz	ε'	ε''	tan δ_e	μ'	μ''	tan δ_m
1	2.42	0.13	0.054	0.96	0.15	0.156
2	2.42	0.11	0.045	0.98	0.11	0.112
2.45	2.41	0.08	0.033	0.99	0.08	0.081
3	2.40	0.05	0.021	1.01	0.08	0.079
4	2.43	0.05	0.021	1.01	0.07	0.069

[a] ε' and ε'' are the real part and imaginary part of complex permittivity, respectively; tan $\delta_e = \varepsilon''/\varepsilon'$ is the dielectric loss tangent; μ' and μ'' are the real part and imaginary part of complex permeability, respectively; tan $\delta_m = \mu''/\mu'$ is the magnetic loss tangent.

Experimental process

In the treatment of the PAM wastewater, a certain amount of CFA_{MW} and 300 mL PAM solution (200 mg L^{-1}) with predetermined pH were added into a beaker (500 mL) successively. The mixture was mixed by mechanical agitation. The degradation of PAM commenced immediately after adding the H_2O_2 solution.

All experiments were conducted at a constant temperature controlled by a water bath (±1 K). At every determined time interval, the mixture was sampled and every sample was pretreated by adding NaOH solution and MnO_2 solid as soon as possible, before filtration. This can stop the generation of $^{\bullet}OH$ and decompose the residual H_2O_2. All the pretreated samples were filtered by vacuum filtration, and all the filtrates were analyzed to determine the TOC and concentration of the leached metallic ions.

In the study of the stability of CFA_{MW}, the separated CFA_{MW} from the treated PAM wastewater was washed by MQ water first

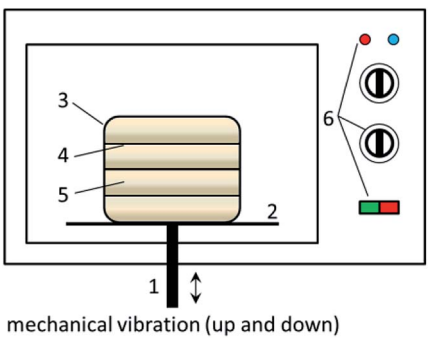

Fig. 1 Schematic for the preparation setup of CFA_{MW} (1) vibratory rod; (2) platform; (3) preparation chamber with multilayers (material: glass; total volume = 1 L); (4) multi-layer plate (material: glass); (5) CFA_R; (6) switch and control knob).

and then dried at 378 K until the weight did not change any more. The CFA_{MW} was used repeatedly under the identical experimental conditions of the first run.

Analytical methods

The TOC in the PAM wastewater was measured by a Rosemount Analytical Dohrmann DC-190 ASM TOC analyzer. The removal rate of TOC was calculated by eqn (2).

$$\text{Removal rate (\%)} = ((c_0 - c)/c_0) \times 100 \quad (2)$$

where, c_0 and c mean the initial concentration of TOC (mg L^{-1}) and the instantaneous concentration of TOC (mg L^{-1}), respectively.

The utilization rate (UR, L mg^{-1}) of H_2O_2 was calculated by eqn (3):

$$UR_{n-m} = (\varphi_m - \varphi_n)/([H_2O_2]_m) - [H_2O_2]_n) \quad (3)$$

where, $[H_2O_2]_m$ and $[H_2O_2]_n$ mean $[H_2O_2] = m$ mg L^{-1} and $[H_2O_2] = n$ mg L^{-1}, respectively. φ_m and φ_n are the removal rates of TOC corresponding $[H_2O_2]_m$ and $[H_2O_2]_n$, respectively, where $n = 0, 4, 8, 12, 16$ corresponding to $m = 4, 8, 12, 16, 20$, one to one.

The life span of $^{\bullet}OH$ in aqueous solution is always very short and it is, therefore, difficult to determine the specific concentration of $^{\bullet}OH$ directly. Thus, a terephthalic acid fluorescence probing technique was applied in this work. Terephthalic acid can capture $^{\bullet}OH$ effectively and generate 2-hydroxyterephtalic acid. The fluorescence intensity of 2-hydroxyterephtalic acid is in proportion to the amount of $^{\bullet}OH$. Terephthalic acid solution was prepared using MQ water according to the literature.[20]

Characterization methods

The surface morphology of CFA_{MW} and CFA_R was observed by scanning electron microscopy (SEM, S4800, Hitachi). The specific surface area and the features of the pores of CFA_{MW} and CFA_R were determined by Brunauer–Emmett–Teller automated analyzer (BET, ASAP 2420, Micromeritics). The crystal structure of CFA_{MW} and CFA_R was determined by X-ray diffraction (XRD, D/max-rB, Rigaku Corporation). The chemical composition of CFA_{MW} and CFA_R was analyzed quantitatively by X-ray fluorescence spectrometry (XRF, ARLADVANT XP+, Thermo electron corporation). The Fourier transform infrared spectrum of CFA_{MW} was measured by FTIR spectrometer (FTIR-650). The concentration of metallic elements in the wastewater was measured by flame atomic absorption spectrometry (PinAAcle 900T, PerkinElmer). The electromagnetic property of CFA_R was measured by Vector Network Analyzers (HP8722ES).

Results and discussion

Optimization of activation condition

The electromagnetic property of CFA_R is given in Table 1, from which it can be seen that both of the imaginary parts (ε'' and μ'') of the complex permittivity and complex permeability are affected by the variation of MW frequency. They always decrease with the increase of frequency. However, the real parts (ε' and μ') of the complex permittivity and complex permeability exhibit insensitivity to the variation of MW frequency. Therefore, the dielectric loss tangent ($\tan\delta_e$) and magnetic loss tangent ($\tan\delta_m$) have the same variation trend with the two imaginary parts. As both of the $\tan\delta_e$ and $\tan\delta_m$ are greater than 1.0×10^{-2} within the range of 1–4 GHz, the CFA_R shows absorbability of MW by means of dielectric loss and magnetic loss.

In this section, the activation condition of CFA_R by MW irradiation (2.45 GHz) was optimized based on the removal rate of TOC in the PAM wastewater. The experiment was arranged according to the orthogonal test ($L_{25}(5^4)$) and the optimum experimental conditions were obtained by the analysis of the average value (I_{ij}, eqn (4)) and the extremum ($R_{E,i}$, eqn (5)) of the TOC removal rate,[21]

$$I_{ij} = \left(\sum_{m=1}^{5} x_{ijm}\right) \Big/ 5 \quad (4)$$

$$R_{E,i} = I_{ij,\max} - I_{ij,\min} \quad (5)$$

where, i, j, and m mean the number of factor, the number of level, and the number of occurrence of (level j of factor i), respectively.

As shown in Table S1,† taking the factor 1 (power of MW) for example, the I_{14} (40.2) has the highest value, while I_{13} (26.0) has the lowest one. Therefore, it can be inferred that 700 W ($j = 4$) of MW power is the optimal value. The same is applicable for each of the other factors (irradiation time, mixing speed, loading of CFA_R). Thus, the optimal experimental conditions are: power of MW = 700 W, irradiation time = 10 min, mixing speed = 120 rpm, and loading of CFA_R = 20 g L^{-1}.

The order of the significance of the four factors can be determined by the comparison of extrema (R_E). As shown in Table S1,† the loading of CFA_R has the most pronounced effect on the removal rate of TOC because of the highest R_E (27.3), while mixing speed has the weakest effect (9.9). The effect of the power of MW and irradiation time occupy the second and third places, respectively. Therefore, the order of significance is: loading of CFA_R > power of MW > irradiation time > mixing speed.

Actually, the above order is in accordance with the property of MW. For a given mixing speed, the MW irradiation can penetrate into the substrate and cause the simultaneous heating of a whole block of material. Therefore, the effect of mixing speed is relatively weaker. For a given irradiation time, the hot-spot effect of the MW irradiation can be produced quickly. Thus, the activation of CFA_R occurs and finishes in a short time. This determines that the irradiation time is relatively less significant as well. As for the power of the MW and the loading of CFA_R, the power of MW can determine the instantaneous temperature of the hot-spot, while more loading of CFA_R will disperse the MW energy, thus causing the decrease of instantaneous temperature of the hot-spot. Therefore, they have an important effect compared with the irradiation time and mixing speed.

Characteristics of CFA_{MW} and CFA_R

Surface morphology. The surface morphology of CFA_R and CFA_{MW} was observed and the components in the special locations were measured by the combination of SEM and EDX. As shown in Fig. 2, the CFA always exhibits uneven surface (Fig. 2A1 and B1) and spheres (Fig. 2A2 and B2) regardless of whether the CFA_R is activated or not. However, the surface morphology of CFA_R has a pronounced variation after MW activation. On focusing the attention on the surface of CFA_R and CFA_{MW}, it can be observed that it is relatively smooth for CFA_R, while many spherical particles are visible on the surface of CFA_{MW}.

The ratio of the components of the elements on the smooth surface and the spherical particles were measured and compared. As shown in Fig. 2C1–C4, the smooth surface (P_1 and P_2) of CFA_R and CFA_{MW} can have the similar ratio of elements, while the main catalytic component (*i.e.*, Fe element) is higher in CFA_{MW} (P_2) than that in CFA_R (P_1). The components in the spherical particles (P_3 and P_4) exhibit remarkable difference. The Fe element on the surface of the spherical particles is much higher than that on the smooth surface, while the Ca element is relatively low. Thus, it can be inferred that the active sites on the surface of the CFA_{MW} are higher than those on CFA_R, which is beneficial for the improvement of the catalytic capacity.

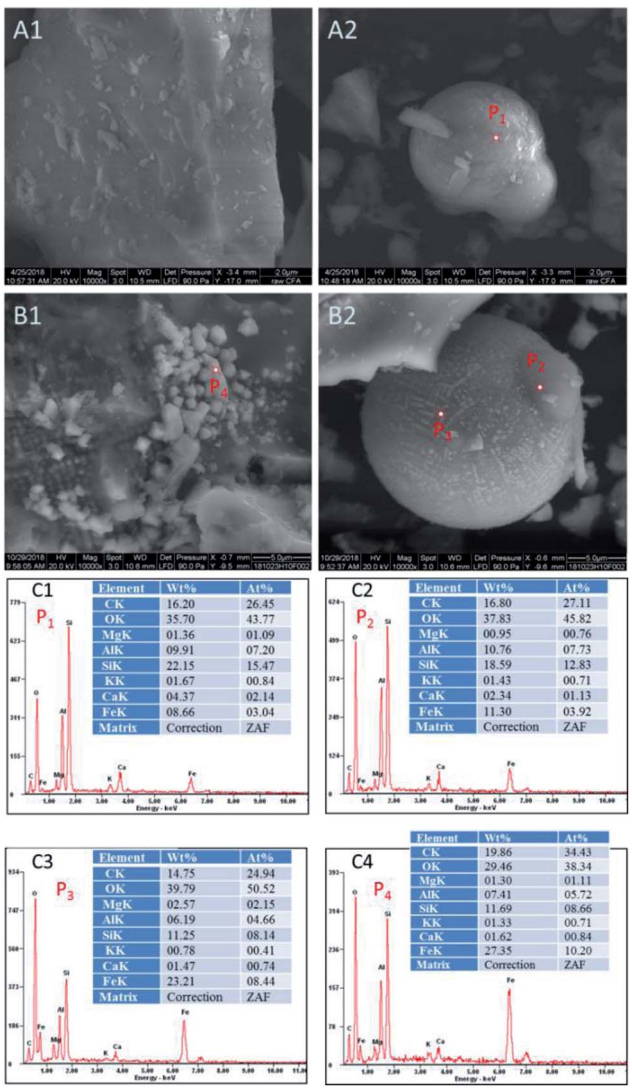

Fig. 2 SEM images and EDX spectra of CFA_{MW} and CFA_R (A1 and A2: SEM of CFA_R; B1 and B2: SEM of CFA_{MW}; C1, C2, C3, and C4: EDX spectra of P_1, P_2, P_3, and P_4).

Table 2 Specific surface area and pore characteristics of CFA_{MW} and CFA_R

Catalyst	Specific surface area ($m^2\ g^{-1}$)	Pore volume ($cm^3\ g^{-1}$)	Average pore diameter (nm)
CFA_{MW}	32.19	0.079	4.79
CFA_R	17.68	0.058	5.76

Specific surface area and pore characteristics. The specific surface areas and pore characteristics of CFA_{MW} and CFA_R were measured and are compared in Table 2. From Table 2, it can be seen that the specific surface area and pore characteristics are significantly different before and after activation. The specific surface area (32.19 $m^2\ g^{-1}$) and pore volume (0.079 $cm^3\ g^{-1}$) of CFA_{MW} is higher than those (17.68 $m^2\ g^{-1}$, 0.058 $cm^3\ g^{-1}$) of CFA_R, while the average pore diameter (4.79 nm) of CFA_{MW} is lower than that of CFA_R (5.76 nm).

Crystalline phase and components of the metallic oxides. The crystalline phase and components of CFA_{MW} was compared with those of CFA_R. The XRD pattern of CFA_{MW} (not given) shows that the primary crystalline phase is mullite ($Al_6Si_2O_{13}$), while quartz (SiO_2), and albite ($(Na, Ca)Al(Si,Al)_3O_8$) occupy the minority. This result is similar with that of CFA_R. Moreover, the components of CFA_{MW} and CFA_R are shown in Table S2,† from which it can be seen that the components are analogous to each other as well.

In essence, it is not difficult to understand this result. The actual temperature on the surface of CFA during the activation process is no more than 573 K, which is much lower than that in the circulating fluidized bed boiler and is not enough to change the crystalline phase. In addition, the variation of the components of the metallic elements will never occur under the MW irradiation. The fluctuation of data is caused by the measurement error.

Functional groups of CFA_{MW}. The FTIR result in Fig. 3 echoes with the result of XRD. The peaks at 795 cm^{-1} and 1086 cm^{-1} represent the anti-symmetric stretching vibration of Si–O–Si, while the peak at 557 cm^{-1} represents the stretching vibration of Al–O in the AlO_6 group.[22,23] The three peaks correspond to the existence of mullite and quartz. The peak at 457 cm^{-1} is the characteristic peak of the bending vibrations of the $[FeO_6]$ group.[24]

It is valuable to notice the stretching vibrations of ˙OH inferred from the peak at 3410 cm^{-1}, which is critical to the catalytic activity of CFA_{MW} due to the formation of ≡Fe–OH (see Fig. 7).

Experimental parameters in the treatment of PAM wastewater

The optimization of the treatment conditions is a critical step in studying the CFA_{MW} catalyzed Fenton-like process. In this work,

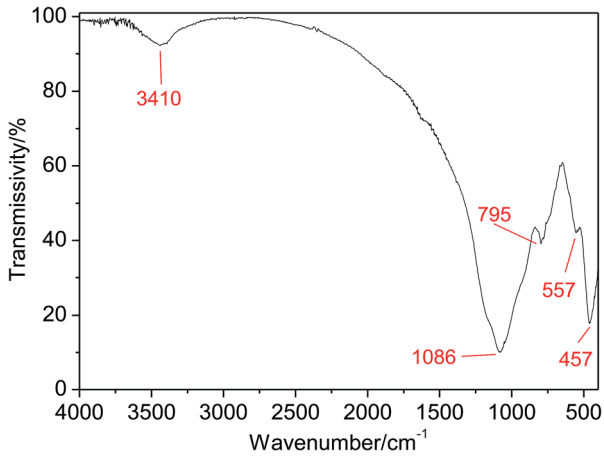

Fig. 3 FTIR spectrum of CFA_{MW}.

H_2O_2 dosage, CFA_{MW} loading, TOC in the PAM wastewater, and the treatment temperature were studied and optimized, respectively.

The data in Fig. 4A shows the effect of H_2O_2 dosage on the TOC removal rate. The removal rate of TOC always increases with the increase of the H_2O_2 dosage. However, it is important to notice that the increase of H_2O_2 dosage from 12 to 20 mg L^{-1} only results in a small growth in the TOC removal rate (from 63.8% to 70.6%) at 50 min. The UR of H_2O_2 in the inset of Fig. 4A shows that more loading of H_2O_2 can cause the rapid decrease of the UR of H_2O_2. When the loading of H_2O_2 is 4 mg L^{-1}, the UR is 10.3 L mg^{-1}, while more loading of H_2O_2 (8 mg L^{-1}) results in the decrease of UR from 10.3 L mg^{-1} to 2.9 L mg^{-1}. Considering the balance of the removal rate of TOC with the UR of H_2O_2, the optimal dosage of H_2O_2 was determined to be 12 mg L^{-1}.

The side reaction occurring in Fenton-like process is responsible for the decline of the UR of H_2O_2. As shown in reaction (6), the excessive loading of H_2O_2 can hinder the reaction between PAM and $^{\cdot}OH$ by the mutual consumption of $^{\cdot}OH$ with H_2O_2.

$$H_2O_2 + {}^{\cdot}OH \rightarrow HO_2{}^{\cdot} + H_2O \quad (6)$$

The data in Fig. 4B shows the effect of CFA_{MW} loading on the TOC removal rate. Similar to the effect of H_2O_2 dosage, with the increase of CFA_{MW} loading, more TOC can be eliminated but it encounters a bottleneck when the CFA_{MW} loading reaches 10 g L^{-1}. More CFA_{MW} loading causes the rapid consumption of H_2O_2 and the rapid generation of $^{\cdot}OH$. Reaction (7) becomes more and more significant with the increase of $^{\cdot}OH$ concentration, *i.e.*, the internal consumption of $^{\cdot}OH$ becomes more severe.

$$2\,{}^{\cdot}OH \rightarrow H_2O_2 \quad (7)$$

The data in Fig. 4C shows the effect of PAM concentration on the TOC removal rate. It can be seen that the increase in PAM concentration has less effect in the range of 50–200 mg L^{-1}, while the effect become substantial when the PAM concentration increases beyond 200 mg L^{-1}. This result can be caused by two reasons. Firstly, the $^{\cdot}OH$ can degrade only a fixed amount of

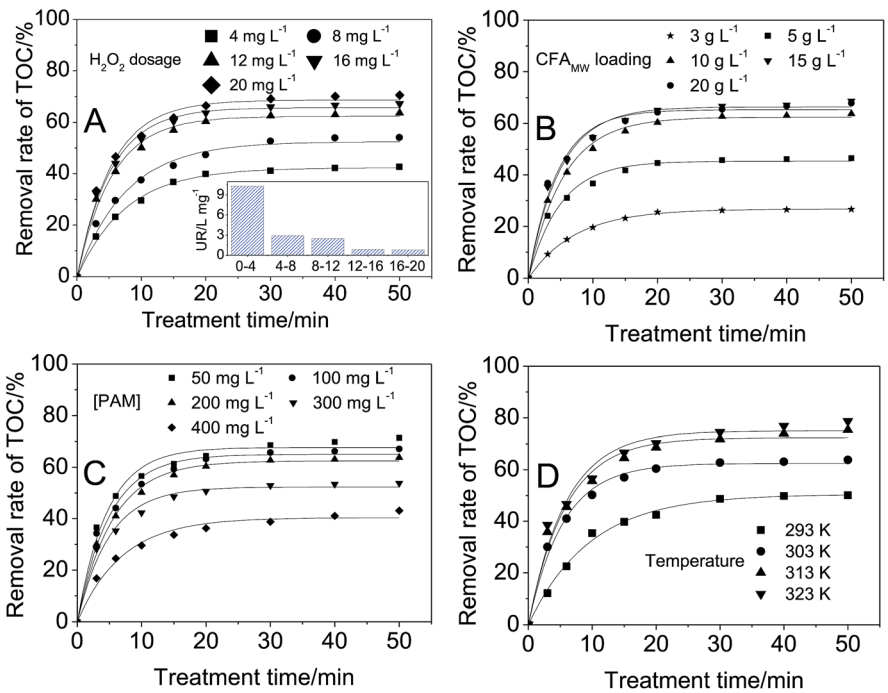

Fig. 4 The effect of experimental conditions on the removal rate of TOC in PAM wastewater. ((A) CFA_{MW} loading = 10 g L^{-1}, [PAM] = 200 mg L^{-1}, T = 303 K, pH = 3; (B) H_2O_2 dosage = 12 mg L^{-1}, [PAM] = 200 mg L^{-1}, T = 303 K, pH = 3; (C) H_2O_2 dosage = 12 mg L^{-1}, CFA_{MW} loading = 10 g L^{-1}, T = 303 K, pH = 3; (D) H_2O_2 dosage = 12 mg L^{-1}, CFA_{MW} loading = 10 g L^{-1}, [PAM] = 200 mg L^{-1}, pH = 3).

PAM, thus more PAM can decrease its removal rate. Secondly, more PAM implies an increase in the viscosity of the wastewater, thus the diffusion of the catalyst H_2O_2 and ·OH is limited seriously even if adequately mixed.

The data in Fig. 4D shows the effect of the wastewater temperature, from which it can be seen that higher temperature encourages in the direction of increasing removal rate of TOC. The removal rate increases from 50.1% to 78.7% at 50 min when the temperature rises from 293 K to 323 K. In this work, 313 K was the optimal value as higher temperature cannot significantly increase the removal rate of TOC.

Kinetic study

The frequently-used pseudo-first order kinetic model is[25]

$$-\mathrm{d}[\mathrm{TOC_R}]/\mathrm{d}t = k_{\mathrm{ap}}\cdot[\mathrm{TOC}]_{\mathrm{R}} \quad (8)$$

where R represents PAM, while $\mathrm{TOC_R}$ means the TOC (mg L^{-1}) of the PAM wastewater, k_{ap} is the pseudo-first order kinetic constant.

However, eqn (8) does not consider the degradation process of PAM and the properties of the degradation products. In reality, the degradation products of organics (including PAM) can always be divided into three kinds, *i.e.*, inorganic matter (H_2O, CO_2, *etc.*), degradable organic matter (intermediates), and non-degradable organic matter.[26] In this section, the generation of the three kinds of products was considered (see eqn (9)) and the corresponding detailed degradation kinetic (DDK) model was derived.

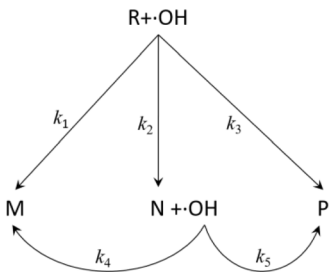

(9)

where k_1, k_2, k_3, k_4, and k_5 are the kinetic constants.

In the DDK model, the initial organic pollutant (R, *i.e.*, PAM) can be degraded by ·OH *via* three paths, *i.e.*, being degraded to non-degradable organic matters (M, k_1), being degraded to intermediates (N, k_2), and being degraded to inorganic matter (P, k_3). Moreover, N can be degraded further by ·OH to M and P, corresponding to the kinetic constants k_4 and k_5, respectively.

Assuming that the five degradation processes follow the pseudo-first kinetics, the DDK model can be described as:

$$-\mathrm{d}[\mathrm{TOC_R}]/\mathrm{d}t = (k_1 + k_2 + k_3)\cdot[\mathrm{TOC}]_{\mathrm{R}} \quad (10)$$

$$-\mathrm{d}[\mathrm{TOC_N}]/\mathrm{d}t = (k_4 + k_5)\cdot[\mathrm{TOC}]_{\mathrm{N}} - k_2\cdot[\mathrm{TOC}]_{\mathrm{R}} \quad (11)$$

$$-\mathrm{d}[\mathrm{TOC_M}]/\mathrm{d}t = -k_1\cdot[\mathrm{TOC}]_{\mathrm{R}} - k_4\cdot[\mathrm{TOC}]_{\mathrm{N}} \quad (12)$$

The TOC of the PAM wastewater can be formulated by the integration of eqn (10)–(12):

$$\begin{aligned}\frac{[\mathrm{TOC}]}{[\mathrm{TOC}]_0} &= \frac{[\mathrm{TOC}]_{\mathrm{R}} + [\mathrm{TOC}]_{\mathrm{N}} + [\mathrm{TOC}]_{\mathrm{M}}}{[\mathrm{TOC}]_{\mathrm{R0}} + [\mathrm{TOC}]_{\mathrm{N0}} + [\mathrm{TOC}]_{\mathrm{M0}}} \\ &= \frac{[\mathrm{TOC}]_{\mathrm{R0}}}{[\mathrm{TOC}]_0}\left(\frac{k_3(k_3+k_2+k_1-k_5-k_4)-k_5k_2}{(k_3+k_2+k_1)(k_3+k_2+k_1-k_5-k_4)}\right. \\ &\quad \times \exp(-(k_3+k_2+k_1)t) \\ &\quad + \frac{k_5k_2}{(k_2+k_4)(k_3+k_2+k_1-k_5-k_4)} \\ &\quad \left.\times \exp(-(k_5+k_4)t) + \frac{k_1(k_5+k_4)+k_4k_2}{(k_3+k_2+k_1)(k_5+k_4)}\right) \\ &\quad + \frac{[\mathrm{TOC}]_{\mathrm{N0}}}{[\mathrm{TOC}]_0}\left(\frac{k_5}{k_5+k_4}\exp(-(k_5+k_4)t) + \frac{k_4}{k_5+k_4}\right) \\ &\quad + \frac{[\mathrm{TOC}]_{\mathrm{M0}}}{[\mathrm{TOC}]_0}\end{aligned} \quad (13)$$

$[\mathrm{TOC}]_{\mathrm{R}}$, $[\mathrm{TOC}]_{\mathrm{N}}$, and $[\mathrm{TOC}]_{\mathrm{M}}$ represent the TOCs of R, N, and M at time t, respectively; $[\mathrm{TOC}]_{\mathrm{R0}}$, $[\mathrm{TOC}]_{\mathrm{N0}}$, and $[\mathrm{TOC}]_{\mathrm{M0}}$ are the initial TOCs of R, N, and M, respectively.

As there is no other chemical substance in the initial PAM wastewater, the initial TOC of M and N is zero. Thus, eqn (13) can be further simplified to eqn (14).

$$\begin{aligned}\frac{[\mathrm{TOC}]}{[\mathrm{TOC}]_0} &= \frac{[\mathrm{TOC}]_{\mathrm{R}} + [\mathrm{TOC}]_{\mathrm{N}} + [\mathrm{TOC}]_{\mathrm{M}}}{[\mathrm{TOC}]_{\mathrm{R0}} + [\mathrm{TOC}]_{\mathrm{N0}} + [\mathrm{TOC}]_{\mathrm{M0}}} \\ &= \frac{[\mathrm{TOC}]_{\mathrm{R0}}}{[\mathrm{TOC}]_0}\left(\frac{k_3(k_3+k_2+k_1-k_5-k_4)-k_5k_2}{(k_3+k_2+k_1)(k_3+k_2+k_1-k_5-k_4)}\right. \\ &\quad \times \exp(-(k_3+k_2+k_1)t) \\ &\quad + \frac{k_5k_2}{(k_2+k_4)(k_3+k_2+k_1-k_5-k_4)} \\ &\quad \left.\times \exp(-(k_5+k_4t) + \frac{k_1(k_5+k_4)+k_4k_2}{(k_3+k_2+k_1)(k_5+k_4)}\right)\end{aligned} \quad (14)$$

The five kinetic parameters in eqn (14) can be obtained by the use of Matlab, based on the multi-variable least-squares method.[2]

The fitting results of k_1, k_2, k_3, k_4, and k_5 under different H_2O_2 dosage, $\mathrm{CFA_{MW}}$ dosage, and PAM concentration are shown in Table 3, from which it can be seen that the regression coefficient (R^2) is always higher than 0.998, thus indicating that the experimental data can follow the DDK model well.

With the increase of the H_2O_2 dosage from 4 to 20 mg L^{-1}, the apparent kinetic constant k_1, k_2, k_3, and k_5 in the DDK model always increase from 0.0891, 0.0536, 0.0636, and 0.0556 min^{-1} to 0.1072, 0.0650, 0.0704, and 0.0665 min^{-1}, respectively. The increase of the above four kinetic constants confirms that PAM can be removed more rapidly due to the generation of more ·OH during the treatment time, while whether the degradation path can be changed cannot be inferred from this result. With the increase of $\mathrm{CFA_{MW}}$ loading from 3 to 20 g L^{-1}, k_1 and k_2 decrease while k_3 and k_5 increase, thus revealing that the primary degradation pathway of PAM shifts towards the direct formation of inorganic matter due to the attack of more ·OH in a short time under the catalysis by more $\mathrm{CFA_{MW}}$. With the increase of PAM concentration from 50 to 400 mg L^{-1}, k_1, k_2, k_3, and k_5 change as well, revealing that the degradation rate is also dependent on the PAM concentration. The increase of k_2 (from 0.0601 to 0.0685 min^{-1}) and the decrease of k_1, k_3, and k_5

Table 3 DDK model parameters calculated from the degradation kinetic analysis of PAM in the CFA_{MW} catalyzed Fenton-like process

H_2O_2 dosage (mg L^{-1})	CFA_{MW} loading (g L^{-1})	PAM concentration (mg L^{-1})	Kinetic constant of the DDK model (min^{-1})					
			k_1	k_2	k_3	k_4	k_5	R^2
4	3	50	0.0891	0.0536	0.0636	0	0.0556	0.9986
12	3	50	0.0904	0.0603	0.0661	0	0.0613	0.9989
20	**3**	50	0.1072	0.0650	0.0704	0	0.0665	0.9991
20	**10**	50	0.0879	0.0626	0.0799	0	0.0701	0.9981
20	**20**	**50**	0.0753	0.0601	0.0856	0	0.0755	0.9992
20	20	**200**	0.0719	0.0644	0.0799	0	0.0638	0.9987
20	20	**400**	0.0678	0.0685	0.0728	0	0.0609	0.9996

implied that the primary degradation pathway of PAM is more towards the formation of intermediates (N), *i.e.*, more PAM is not degraded completely. The value of k_4 is always kept at zero, showing that the degradation path of N to M was not manifested.

Features of CFA_{MW} catalyzed Fenton-like process

Optimal pH range. In the classic Fenton process, the optimum range of pH is always fixed at 3,[27] thus limiting the application of the Fenton process in industry. Thus, widening the pH range is important to break the limitation. In this section, the optimal pH range of the Fenton-like process was investigated to examine whether the CFA_{MW} has advantage in this aspect.

As shown in Fig. 5, when pH varies in the range of 2–5, the removal rate of TOC varies in a small range (64.6–70.5%) at 50 min. Raising the pH further causes a remarkable decrease of the removal rate of TOC, revealing that the optimal range of pH is 2–5. This range is not very wide but has shown progress compared with that (pH = 3) of the classic Fenton process.

The difference in the pH range could be caused by the different properties of the catalysts. The performance of Fe^{2+} in the Fenton process is affected significantly by pH. A pH higher than 3 can cause the oxidation of Fe^{2+} and precipitation in the form of $Fe(OH)_3$, resulting in the deactivation of Fe^{2+}. Relatively speaking, the effect of pH on the surface of CFA_{MW} is weaker. The active sites on the surface of CFA_{MW} always contain Fe_2O_3,

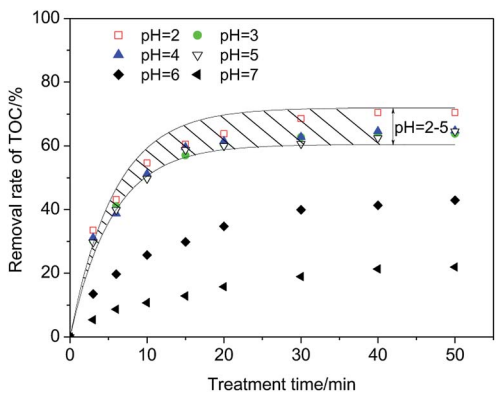

Fig. 5 Optimal range of pH in the CFA_{MW} catalyzed Fenton-like process (H_2O_2 dosage = 12 mg L^{-1}, CFA_{MW} loading = 10 g L^{-1}, [PAM] = 200 mg L^{-1}, T = 313 K).

which have been oxidized to +3. The catalytic process of the active sites is different from Fe^{2+} and the OH^- has a relatively weak effect on the catalytic mechanism.

Investigation of $^{\bullet}OH$ in different oxidation systems. The relative amount of $^{\bullet}OH$ generated in different Fenton-like processes were compared. As shown in Fig. 6, it can be observed intuitively that Fe^{3+}–H_2O_2 and CFA_R–H_2O_2 systems generate a lesser amount of $^{\bullet}OH$ than that of another two systems. In the Fe^{3+}–H_2O_2 system, the Fe^{3+} needs to be reduced to Fe^{2+} first before generating $^{\bullet}OH$. However, the reduction reaction of Fe^{3+} (eqn (15)) is the rate controlled step (k = 0.01–0.02 L mol^{-1} s^{-1}).[28]

$$Fe^{3+} + H_2O_2 \rightarrow Fe^{2+} + HO_2^{\bullet} + H^+ \quad (15)$$

In the CFA_R–H_2O_2 system, the active sites are relatively lesser in number because they may be covered by other minerals or inactive oxides.

When focussing attention on the Fe^{2+}–H_2O_2 and CFA_{MW}–H_2O_2 systems, it is interesting that the amount of $^{\bullet}OH$ generated in the Fe^{2+}–H_2O_2 system is more in the prophase of the reaction (at 5 min) but lesser in the later stage of the reaction (at 10 and 15 min) (see Fig. 6). This result indicates the different advantages reflected by the Fe^{2+}–H_2O_2 system and the CFA_{MW}-system. As for the Fe^{2+}–H_2O_2 system, Fe^{2+} can have a better catalytic capacity than CFA_{MW}. This is the primary reason that more $^{\bullet}OH$ can be generated before 5 min. However, as the reaction proceeds, Fe^{2+} gets oxidized to Fe^{3+} rapidly but Fe^{3+} cannot be reduced to Fe^{2+} in time. Thus, the amount of $^{\bullet}OH$ generated reaches a platform with a gentle slope. As for the CFA_{MW}–H_2O_2 system, CFA_{MW} can have a better catalytic persistence than Fe^{2+}, resulting in the amount of $^{\bullet}OH$ generated that catches up with and exceeds that of the Fe^{2+}–H_2O_2 system at the later stage.

The importance of $^{\bullet}OH$ was compared with other free radicals (*i.e.*, $^{\bullet}HO_2/^{\bullet}O_2^-$) in the CFA_{MW}–H_2O_2 system. *n*-Butanol and benzoquinone were applied to scavenge $^{\bullet}OH$ and $^{\bullet}HO_2/^{\bullet}O_2^-$, respectively.[29] Under the optimal treatment conditions of the wastewater (75.3% of TOC removal rate), the removal rate of TOC (17.6%) has a remarkable decline in the presence of *n*-butanol, while 64.1% of TOC can still be removed in the presence of benzoquinone, revealing the $^{\bullet}OH$ play a primary role in the CFA_{MW}–H_2O_2 system, while $^{\bullet}HO_2/^{\bullet}O_2^-$ play the auxiliary role.

Leachability and stability of CFA_{MW}. From Table S2,† it can be inferred that the use of CFA_{MW} may introduce heavy metallic and toxic elements into treated wastewater such as Fe, Cr, Mn, Ni, and Cu. These elements may cause secondary water

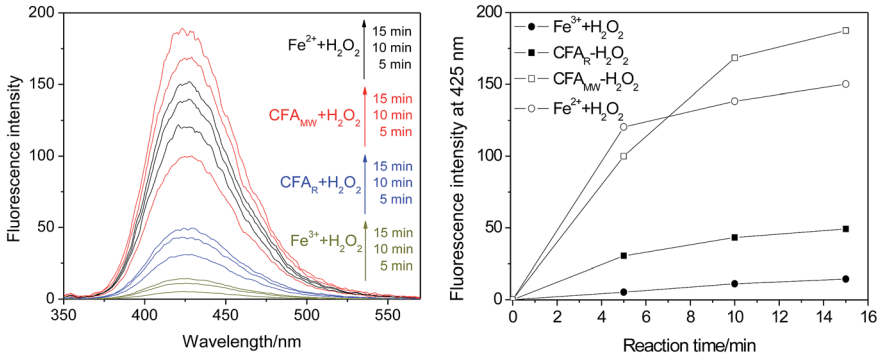

Fig. 6 Comparison of the relative generation amount of $^{\bullet}OH$ in different Fenton-like processes. (H_2O_2 dosage = 12 mg L^{-1}, [PAM] = 200 mg L^{-1}, T = 313 K, pH = 3. For the CFA_{MW}–H_2O_2 system and CFA_R–H_2O_2 system, CFA_{MW} loading = CFA_R loading = 10 g L^{-1}. For the Fe^{2+} + H_2O_2 system and Fe^{3+}–H_2O_2 system, [Fe^{2+}] = [Fe^{3+}] = 445 mg L^{-1}, which is equivalent to the 10 g L^{-1} CFA_{MW} loading).

pollution. Thus, the leachability of these elements from CFA_{MW} must be considered before industrial application. As shown in Table 4, nine primary elements were detected. Fortunately, the leaching amount of each element in the 1st run is lower than the Chinese standard (GB8978-1996). Meanwhile, the leaching amount of these elements always decreases in the successive five runs, revealing the possibility of direct use of CFA_{MW} in the treatment of PAM-contaminated wastewater.

While the test of the leachability can indicate the possibility of use of CFA_{MW} in the industry from the perspective of environmental protection, the test of stability indicates the economic feasibility. As shown in Fig. S1,† it can be observed that the removal rate of TOC always decreases with the increase in run time (from 63.8% to 52.8%), revealing the loss of the catalytic capacity of CFA_{MW}. This could be caused by the dissolution and loss of the active metallic elements.

This decline of catalytic capacity is common in these studies. As shown in Table S3,† all listed catalysts cannot be used continuously but have a limited run time. The comparison of these catalysts should be conducted on different aspects. The preparation condition of a catalyst is a significantly effective parameter, and a simple and cheap preparation method can decrease the cost of wastewater treatment remarkably. This is the advantage of CFA_{MW} because it was prepared by a single step physical method, *i.e.*, MW irradiation, while other catalysts were prepared by multi-step processes where calcination and chemical reagents were always used. As for the stability and the minimum treatment efficiency, they can mutually affect the efficiency of the catalyst. The catalyst may be reused more times when the minimum treatment efficiency is not limited strictly, whereas it needs to be replaced frequently in a harsher working condition (see Table S3†). Thus, it is more appropriate to compare the stability of different catalysts in identical conditions.

Proposed catalytic mechanism of CFA_{MW}

The catalytic mechanism associated with Fe element is shown in Fig. 7. It can be seen that the trivalent Fe on the surface of CFA_{MW} (≡Fe(III)–OH) can be reduced to divalent Fe (≡Fe(II)) through two paths, namely, on reacting with H_2O_2 (path I) and reacting with $^{\bullet}HO_2/^{\bullet}O_2^-$ (path II). Among the two paths, path I is the main one as H_2O_2 has an external source (artificial input), while the generation of $^{\bullet}HO_2/^{\bullet}O_2^-$ is accompanied by the consumption of ≡Fe(II) and $(H_2O_2)_s$ (path III and IV).

Despite the mechanism in Fig. 7 that gives a detailed catalytic path, it is only associated with Fe catalysis and could only be a part of the complicated mechanism in the CFA_{MW}-catalyzed Fenton-like process. Some metallic elements existing in CFA_{MW} (besides Fe) have been reported as additives in the Fe-base Fenton-like catalysis, such as Mn, Ni, Co, Cu, Nb, and V.[30–35] Thus, the adjunct catalysis from these elements must be considered. In reality, these metallic elements have two adjunct catalytic paths, *i.e.*, (I) promoting the generation of active species that have oxidation capacity, and (II) promoting the transfer of electron.

As for the generation of the active species, beside the Fe element, the above listed metallic elements can generate $^{\bullet}OH$ *via* the Haber–Weiss path as well.[36] Taking the V element for instance, the catalytic process is shown in eqn (16)–(18).

$$V(IV) + O_2 \rightarrow V(V) + O_2^- \quad (16)$$

$$O_2^- + O_2^- + 2H^+ \rightarrow H_2O_2 + O_2 \quad (17)$$

$$H_2O_2 + V(IV) \rightarrow OH^- + {}^{\bullet}OH + V(V) \quad (18)$$

As for the transfer of electron, different metallic oxides can affect each other by the oxidation–reduction reactions. This can

Table 4 Concentration (mg L^{-1}) of the leached elements from CFA_{MW} in the Fenton-like process (CFA_{MW} loading = 10 g L^{-1})

Metallic element	Fe	Al	Ti	Cr	Mn	Ni	Cu	Nb	Ca
1st run	0.557	0.202	0.058	0.032	0.094	0.011	0.019	0.006	0.157
3rd run	0.461	0.158	0.037	0.031	0.075	0.085	0.011	0.005	0.112
5th run	0.409	0.126	0.021	0.023	0.068	0.059	0.007	—	0.067

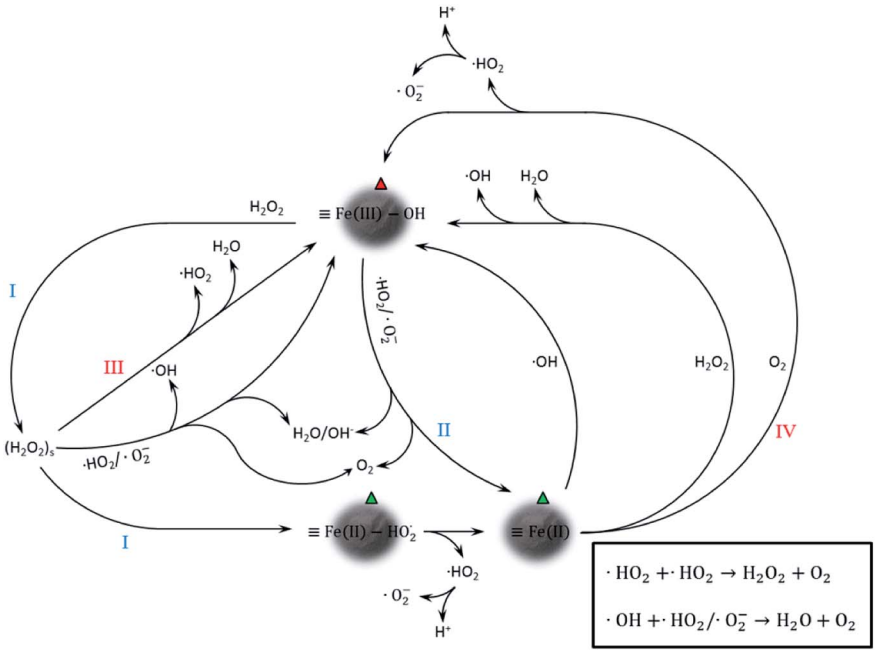

Fig. 7 Proposed catalytic mechanism of CFA_{MW} in the heterogeneous Fenton-like process.

promote the recycling of B^{n+x}/B^n ($n \geq 1$, $x \geq 1$), which is critical for the Fenton-like process.

According to the statement above, the heterogeneous catalytic mechanism of CFA_{MW} is actually very complicated because of the mutual effect of the different metallic elements. The detailed mechanism still needs more profound study.

Finally, it has to be noted that the mechanism stated above is based on the surface catalysis, where H_2O_2 must spread to the surface of CFA_{MW} first before the catalysis by the active sites. However, according to the results in the section "Investigation of ˙OH in different oxidation systems", the catalysis by the dissolved metallic elements should be considered as well. Thus, the catalysis by CFA_{MW} is a multi-metal catalytic and two-phase process.

Conclusions

MW irradiation can activate the catalytic potential of the CFA_R effectively.

(I) The most significant factor in the activation process is the CFA_R loading, while the importance of the MW power, irradiation time, and mixing speed decline in this sequence. During the MW irradiation, the surface morphology of the CFA_R can be changed, and the specific surface area and the pore volume of CFA_R can be increased significantly.

(II) In the treatment of the PAM wastewater by CFA_{MW}-catalyzed Fenton-like process, more than 75% of the TOC can be eliminated under the optimal conditions ($[H_2O_2] = 12$ mg L^{-1}, CFA_{MW} loading $= 10$ g L^{-1}, $[PAM] = 200$ mg L^{-1}, $T = 313$ K). The variation in the CFA_{MW} loading and PAM concentration can change the degradation path of PAM, while the increase in the H_2O_2 dosage can only accelerate the degradation of PAM.

(III) The CFA_{MW} can widen the optimal pH range of the classic Fenton process from 3 to 2–5. Moreover, the CFA_{MW} has better catalytic persistence than that of Fe^{2+} but less catalytic capacity. The leaching of heavy metallic/toxic elements is lower than the limits of the GB8978-1996 standard but it still weakens the stability of CFA_{MW}. The anti-leaching study directed for CFA_{MW} could be promising from the standpoint of industrial application.

(IV) The Fe(III)–OH on the surface of CFA_{MW} contributes to the primary heterogeneous catalytic capacity, while other metallic elements play a role by accelerating the generation of ˙OH and the redox reaction of Fe(III)/Fe(II). The homogeneous catalysis caused by the leached metallic elements cannot be overlooked as well.

Conflicts of interest

There are no conflicts to declare.

Acknowledgements

This work was supported by the National Natural Science Foundation of China (grant number 51808039); Science and Technology Projects of Beijing Municipal Education Commission (grant number KM201910017008); National Innovation and Entrepreneurship Training Program for students (grant number 18010282001/005).

References

1 J. Anotal, N. Wasukran and N. Boonrattanakij, *Chem. Eng. J.*, 2018, **352**, 247–254.

2 N. N. Wang, T. Zheng, J. P. Jiang and P. Wang, *Chem. Eng. J.*, 2015, **260**, 386–392.
3 W. Leal, L. A. Lourenco, H. D. Brandao, A. da Silva, S. M. A. G. U. de Souza and A. A. U. de Souza, *J. Hazard. Mater.*, 2018, **359**, 96–103.
4 L. Clarizia, D. Russo, I. Di Somma, R. Marotta and R. Andreozzi, *Appl. Catal., B*, 2017, **209**, 358–371.
5 J. Zhang, S. Q. Wu, W. J. Bi, X. F. Zhao and G. D. Liu, *Mater. Lett.*, 2019, **234**, 13–16.
6 C. di Luca, P. Massa, J. M. Grau, S. G. Marchetti, R. Fenoglio and P. Haure, *Appl. Catal., B*, 2018, **237**, 110–1123.
7 T. P. H. Ngo and T. K. Le, *J. Sol-Gel Sci. Technol.*, 2018, **88**, 211–219.
8 Y. Y. Zhou, X. C. Liu, Y. Q. Zhao, S. Luo, L. L. Wang, Y. Yang, M. A. Oturan and Y. Mu, *J. Catal.*, 2018, **365**, 184–194.
9 C. Y. Su, W. G. Li, X. Z. Liu, X. F. Huang and X. D. Yu, *Front. Environ. Sci. Eng.*, 2016, **10**, 37–45.
10 S. Jauhar and S. Singhal, *Ceram. Int.*, 2014, **40**, 11845–11855.
11 J. Gao, L. Wu, S. J. Liang, S. L. Zhang, P. Liu and X. Z. Fu, *Chin. J. Catal.*, 2010, **31**, 317–321.
12 A. A. S. Tigue, R. A. J. Malenab, J. R. Dungca, D. E. C. Yu and M. A. B Promentilla, *Minerals*, 2018, **8**, 411.
13 N. N. Wang, L. L. Hao, J. Q. Chen, Q. Zhao and H. Xu, *Environ. Sci. Pollut. Res.*, 2018, **25**, 12481–12490.
14 S. B. Yang, G. L. Song, Y. J. Na and Z. Yang, *Appl. Therm. Eng.*, 2018, **141**, 29–41.
15 O. Z. Ozdemir and S. Piskin, *Waste Biomass Valorization*, 2019, **10**, 143–154.
16 Y. B. Huang, J. S. Qian and J. Y. Zhang, *J. Build. Mater.*, 2010, **13**, 291–294.
17 S. Deng, P. Wang, G. S. Zhang and Y. Dou, *J. Hazard. Mater.*, 2016, **307**, 64–72.
18 G. C. Liu, L. Li, L. P. Qiu, S. L. Yu, P. Liu, Y. B. Zhu, J. Hu, Z. Y. Liu, D. S. Zhao and H. J. Yang, *J. Membr. Sci.*, 2018, **545**, 348–357.
19 T. Zheng, *J. Water Reuse Desalin.*, 2017, **7**, 378–386.
20 J. G. Yu, W. G. Wang, B. Cheng and B. L. Su, *J. Phys. Chem. C*, 2009, **113**, 6743–6750.
21 R. H. G. Ranil, H. M. L. Niran, M. Plazas, R. M. Fonseka, H. H. Fonseka, S. Vilanova, I. Andujar, P. Gramazio, A. Fita and J. Prohens, *Sci. Hortic.*, 2015, **193**, 174–181.
22 S. Sivalingam and S. Sen, *Appl. Surf. Sci.*, 2018, **455**, 903–910.
23 R. Kaur and D. Goyal, *J. Mater. Cycles Waste Manage.*, 2016, **18**, 186–200.
24 M. E. Kalaw, A. Culaba, H. Hinode, W. Kurniawan, S. Gallardo and M. A. Promentilla, *Materials*, 2016, **9**, 580.
25 L. M. Hu, G. S. Zhang, M. Liu, Q. Wang and P. Wang, *Chem. Eng. J.*, 2018, **338**, 300–310.
26 J. A. Giroto, A. C. S. C. Teixeira, C. A. O. Nascimento and R. Guardani, *Chem. Eng. Process.*, 2008, **47**, 2361–2369.
27 S. Li, G. S. Zhang, P. Wang, H. S. Zheng and Y. J. Zheng, *Chem. Eng. J.*, 2016, **294**, 371–379.
28 J. H. Ramirez, F. M. Duarte, F. G. Martins, C. A. Costa and L. M. Madeira, *Chem. Eng. J.*, 2009, **148**, 394–404.
29 H. Liwei, W. Liguo, R. Sébastien and Z. Hui, *J. Hazard. Mater.*, 2016, **302**, 458–467.
30 Q. Wang, X. F. Wang and B. Tian, *Water Sci. Technol.*, 2018, **77**, 2772–2780.
31 Y. J. Yao, H. Chen, C. Lian, F. Y. Wei, D. W. Zhang, G. D. Wu, B. J. Chen and S. B. Wang, *J. Hazard. Mater.*, 2016, **314**, 129–139.
32 Y. C. Wang, S. Shia, C. Wang and S. Fanga, *Environ. Prot. Eng.*, 2018, **44**, 131–145.
33 C. M. Zheng, C. W. Yang, X. Z. Cheng, S. C. Xu, Z. P. Fan, G. H. Wang, S. B. Wang, X. F. Guan and X. H. Sun, *Sep. Purif. Technol.*, 2017, **189**, 357–365.
34 Z. Jia, S. X. Liang, W. C. Zhang, W. M. Wang, C. Yang and L. C. Zhang, *J. Taiwan Inst. Chem. Eng.*, 2017, **71**, 128–136.
35 Y. Y. Zhang, J. H. Deng, C. He, S. S. Huang, S. H. Tian and Y. Xiong, *Environ. Technol.*, 2010, **31**, 145–154.
36 Z. J. Song, B. Wang, J. Yu, C. Ma, T. Chen, W. Yang, S. Liu and L. S. Sun, *Chem. Eng. J.*, 2018, **354**, 517–524.